JOURNAL OF MATERIALS SCIENCE 21 (1986) 2721–2730

The constitution of the Ni–Al–Ru system

S. CHAKRAVORTY, D. R. F. WEST
Department of Metallurgy and Materials Science, Imperial College, London SW7 2BT, UK

The constitution of the Ni–Al–Ru system has been investigated in the range 0 to ~50 at% Al. Isothermal sections at 1523 and 1273 K have been determined using microstructural observations, electron probe microanalysis and X-ray diffraction. The phases present were: nickel-based solid solution (γ); γ' (based on Ni_3Al); solid solutions based on NiAl and RuAl, respectively (designated β_1 and β_2), and ruthenium-based solid solution (Ru). The maximum solubility of Ru in γ' was ~5 at%. β_1 and β_2 show extensive range of solubilities, namely up to ~20 at% Ru in β_1 and up to ~25 to 35 at% Ni in β_2. Three-phase equilibrium between γ, β_2 and (Ru) existed at 1523 and 1273 K. Also at 1523 K, three-phase equilibria existed between γ, γ' and β_1 and γ, β_1 and β_2, while at 1273 K, the equilibria were between γ', β_1, β_2 and γ, γ', β_2 indicating the occurrence of a reaction $\gamma + \beta_1 \rightarrow \gamma' + \beta_2$ at a temperature between 1523 and 1273 K. Liquidus features have been deduced from data on as-solidified structures. Lattice parameter data and hardnesses are also reported.

1. Introduction

The results reported here derive from a research programme aimed to determine the influence of platinum group metals (PGMs) on the constitution of nickel-based superalloys. Platinum has found an important role in platinum–aluminide coatings, conferring improved protection in high temperature service [1, 2]. Also, PGMs have proved of interest in seeking improvements in M–Cr–Al–Y coatings [3] and as additions to nickel-based alloys to enhance properties [4–6].

Ni–Al–X systems (where X is a PGM), containing up to ~50 at % Al form a convenient basis for constitutional studies. The present paper is concerned with the Ni–Al–Ru system at 1523 and 1273 K, together with observations on the solidification behaviour. In this system a feature of potential interest in relation to coatings technology is the alloying behaviour of the NiAl (β) phase with respect to ruthenium additions. Among the PGMs ruthenium has the attraction of relatively low cost.

2. Literature survey

The binary Ni–Al system has been extensively studied [7–10]: the key features relevant to the present work involving γ, γ' and β (NiAl) are well established. γ' forms by a peritectic reaction: $L + \beta \rightarrow \gamma'$ at 1668 K and there is a eutectic reaction: $L \rightarrow \gamma + \gamma'$ at 1658 K. γ' shows a significant range of stoichiometry, e.g. from ~23 to 28 at % Al at 1500 K. At the stoichiometric composition the lattice parameter of the $L1_2$ structure is 0.3570 nm. β phase melts congruently at 1911 K and has a very wide range of stoichiometry, e.g. from ~33 to 57 at % Al at 1500 K. The crystal structure is of the CsCl(B2) type and the lattice parameter shows a maximum value of 0.2887 nm at stoichiometry. The β-phase takes part in the peritectic reaction: $L + \beta \rightarrow Ni_2Al_3$ at 1406 K. The structure of Ni_2Al_3 is hexagonal ($D5_{13}$) with $a = 0.4036$ nm, $c = 0.4900$ nm, $c/a = 1.214$ [11].

In the Ni–Ru system which has been recently reviewed [12], there is extensive solubility of ruthenium in nickel (i.e. γ-phase) and also of nickel in ruthenium; the latter solid solution is designated here as (Ru). A peritectic reaction $L + (Ru) \rightarrow \gamma$ occurs at 1823 K, at which temperature γ contains ~34 at % Ru and (Ru) contains ~48 at % Ni; the solid solubilities in γ and (Ru) decrease markedly with temperature. A metastable intermediate phase, designated η, having a tetragonal structure $a = 0.451\,06$ nm and $c = 0.362\,016$ nm has been found in rapidly solidified Ni–Ru alloys containing 30 to 40 at % Ru [13].

In the Ru–Al system which contains a series of intermetallic compounds RuAl is a major interest in the present context. It has the same structure as NiAl, i.e. (B2) type with the lattice parameter reported as 0.303 nm [14, 15] or 0.295 nm [16]. Melting of RuAl occurs congruently at ~2300 K, and there is a eutectic: $L \rightarrow RuAl + (Ru)$ at ~2193 K; at ~1500 K RuAl shows a range of stoichiometry from ~48 to 56 at % Al. In the compositional range involving higher Al contents the compound Ru_2Al_3 forms at 1870 K by the reaction: $L + RuAl \rightarrow Ru_2Al_3$. Ru_2Al_3 has been reported as having the same hexagonal structure as Ni_2Al_3 with $a = 0.405$ to 0.407 nm, $c = 0.519$ to 0.537 nm, $c/a = 1.22$ to 1.32 [14, 15]. Other work reports Ru_2Al_3 as tetragonal: $a = 0.3079$, $c = 1.433$, $c/a = 4.65$ [17]. At 1270 K, Ru_2Al_3 decomposes eutectoidally to form $RuAl + RuAl_2$.

An investigation has been reported of the complete isothermal section of the Ni–Al–Ru system at 823 K [18]. Alloys prepared from high purity materials were annealed at 823 K for 1400 h; in the case of nickel-rich samples this treatment was preceded by annealing at 1273 K for 700 h. X-ray diffraction and metallography

0022–2461/86 $03.00 + .12

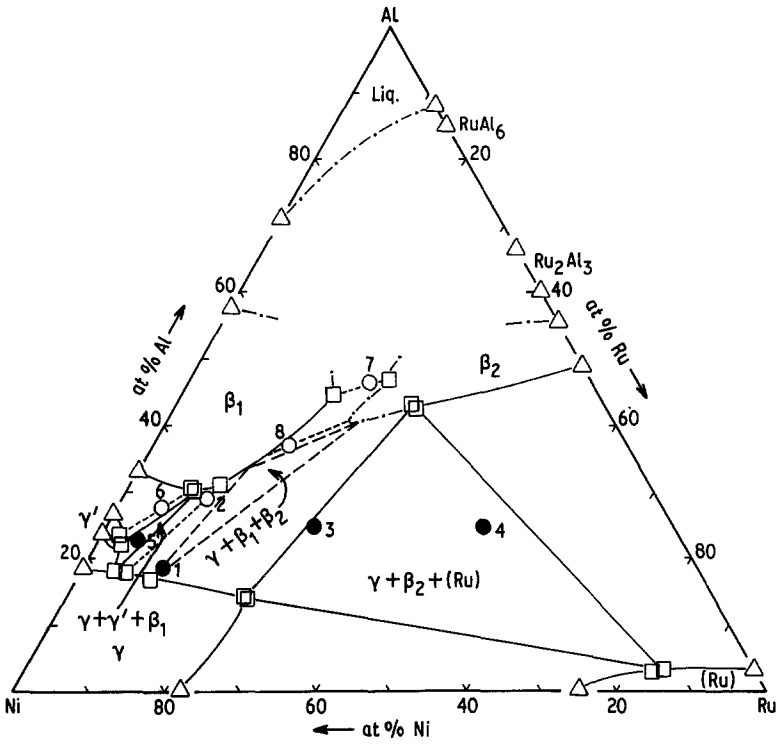

Figure 1 Partial isothermal section of the Ni–Al–Ru system at 1523 K. (□) phase composition by EPMA. (△) data from previous work [7–10, 12, 14–16]. (-----) tie-line determined by EPMA (except for alloy 8 at 1523 K, where it is estimated). (–·–·–) extrapolated/interpolated phase boundaries (see text). (– – –) interpolated three-phase regions. (——) tie-triangle determined by EPMA. (○), composition of 2 phase alloy. (●), composition of 3 phase alloy.

were used to study the phase equilibria. Among features of interest for the composition range of the present work, negligible solubility of ruthenium in Ni_3Al was reported; also a solubility gap between NiAl and RuAl was found, the maximum solubility of ruthenium in NiAl being ~5 at % and that of nickel in RuAl being ~8 at %. The following three-phase equilibria were found: $\gamma + \gamma' +$ NiAl, $\gamma +$ NiAl + RuAl and $\gamma +$ RuAl + (Ru). No ternary compounds were reported in the system.

Recent work has been reported on the Ni_3Al–Ni_3Cr–Ni_3Ru section of the Ni–Cr–Al–Ru system at 1523 and 1273 K [19]. The solubility of chromium and ruthenium in γ' was found to total ~4 at %. γ/γ' lattice parameter mismatch values were between ~0.08 and 0.39%. In schematic representations of the system the assumption was made of complete mutual solid solubility between NiAl and RuAl, but evidence to support this assumption was not obtained.

3. Experimental procedure

Eight ternary alloys were prepared (Table I) of which alloys 1 to 5, with Al contents from ~18 to 30 at % and ruthenium contents from 2 to 6 at % were chosen to determine the γ, γ' and β(NiAl) equilibria. Alloys 3 and 4 of higher ruthenium content were selected to explore equilibria involving (Ru), while alloys 7 and 8 of high aluminium content were designed to elucidate the NiAl–RuAl relationships [20].

High purity metals: Ni (99.99%), Al (99.99%), Ru (~99.9%) were used to make arc-melted ingots of ~10 g weight; several remelts were made to assist in achieving homogeneity. The melting losses were generally < 1% except for alloys 7 and 8 where the losses were higher (Table II).

Portions of the ingots were cut for investigation of the as-solidified condition. The remaining portions were sealed in silica tube under a partial pressure of argon for annealing; in all cases annealing was followed by quenching in iced water (WQ). Alloys 1 to 4 were annealed for 10 days at 1523 K and portions were then further annealed for 10 days at 1273 K. Alloys 5 to 8 were annealed for 5 days at 1563 K, furnace cooled to 1523 K and held for 14 days; portions were then further annealed for 28 days at 1273 K. The temperature control was ~ ±5 K.

Light microscopy and scanning electron microscopy were carried out. Etching was done either with a mixture of 2% HF, 10% HNO_3 in water, or electrolytically at 6 V with an aqueous solution of 10% NaOH. Tie-line and tie-triangle compositional data were determined by electron probe microanalysis (EPMA) using a JEOL JSM-35CF instrument with LINK system software; the relative error of the analysis was typically up to ~ ±1% of the individual elements. The attainment of local equilibrium was indicated by the absence of detectable concentration gradients in phase particles.

The lattice parameters of phases were determined by X-ray diffractometry of polished, bulk samples; a graphite monochromator with Cu$K\alpha$ radiation with a specimen spinner were used. The accuracy of the measured parameters was estimated as ~ ±0.2%.

4. Results and discussion

Tables I and II show data for phase compositions, lattice parameters and hardness for the as-solidified and annealed alloys. Figs 1 and 2 show isothermal sections at 1523 and 1273 K, while Fig. 3 represents information from as-solidified alloys with a possible liquidus projection. Microstructural features are illustrated in Figs 4 to 6 and 8 to 13.

The phases encountered were γ, γ', (Ru) and solid solutions based on NiAl and RuAl, respectively, designated here as β_1 and β_2. Some details of the identification of the β_1 and β_2 phases and their composition ranges have been reported elsewhere [20].

TABLE I Nominal alloy compositions, hardness values, experimental and calculated lattice parameters (nm)

Alloy no.	Nominal alloy composition (at %) Ni–Al–Ru	Treatment	Hardness (H_v)	Phases present	Structure of phases present and lattice parameter (nm)				
					γ, fcc, a	γ' (based Ni_3Al), Ll_2 cubic, a	β_1 (based on NiAl), B2 (CsCl) cubic, a	β_2 (based on RuAl), B2 (CsCl) cubic, a	(Ru), Hex a / c
1	70–20–10	As-solidified	318	$\gamma + \gamma' + \beta_1$	0.3594 [0.3576]	0.3581	0.2890		
		1523 K	274	$\gamma + (\gamma') + \beta_1 + \beta_2$	0.3589 [0.3573]	0.3584	0.2899	0.2921‡ [0.2921]	
		1273 K	284	$\gamma + \gamma' + \beta_2$	0.3584 [0.3570]	0.3575 [0.3576]		0.2946 [0.2945]	
2	60–30–10	As-solidified	655	$\gamma' + \beta_1 + \beta_2$		0.3579 [0.3581]	0.2880 [0.2871]	0.2920† [0.2926]	
		1523 K*	642	$\gamma + (\gamma') + \beta_1$	0.3576 [0.3569]	0.3573	0.2878 [0.2871]		
		1273 K	433	$\gamma' + \beta_2$		0.3576 [0.3577]		0.2947 [0.2945]	
3	50–25–25	As-solidified	515	$\gamma + \beta_2$	0.3636 [0.3627]			0.2937 [0.2946]	
		1523 K	414	$\gamma + \beta_2 + (Ru)$	0.3635 [0.3606]			0.2945 [0.2942]	§
		1273 K	489	$\gamma + \beta_2 + (Ru)$	0.3597 [0.3581]			0.2947 [0.2945]	0.2696 (c/a = 1.586) 0.4276
4	25–25–50	As-solidified	882	$\gamma + \beta_2 + (Ru)$	0.3642 [0.3634]			0.2958 [0.2960]	0.2659 (c/a = 1.603) 0.4262
		1523 K	773	$\gamma + \beta_2 + (Ru)$	0.3638 [0.3608]			0.2947 [0.2944]	0.2687 (c/a = 1.591) 0.4276
		1273 K	689	$\gamma + \beta_2 + (Ru)$	0.3600 [0.3581]			0.2949 [0.2947]	0.2693 (c/a = 1.588) 0.4277
5	72–23–5	As-solidified	360	$\gamma' + \beta_1$		0.3573 [0.3576]	0.2881 [0.2857]		
		1523 K	294	$\gamma + \gamma' + \beta_1$	0.3574 [0.3566]	0.3577 [0.3573]	0.2874 [0.2863]		
		1273 K	222	$\gamma' + \beta_2$		0.3575 [0.3577]		0.2946 [0.2946]	
6	67–28–5	As-solidified	583	$\gamma' + \beta_1$		0.3571 [0.3572]	0.2897 [0.2854]		
		1523 K	388	$\gamma' + \beta_1$		0.3575 [0.3573]	0.2873 [0.2863]		
		1273 K	302	$\gamma' + \beta_2$		0.3574 [0.3576]		0.2945 [0.2944]	
7	28–50–22	As-solidified	770	$\gamma' + \beta_1 + \beta_2$		0.3594 [0.3574]	0.2901 [0.2900]	0.2944 [0.2942]	
		1523 K	796	$\beta_1 + \beta_2$			0.2936 [0.2921]	0.2942 [0.2937]	
		1273 K	820	$\beta_1 + \beta_2$			0.2931 [0.2923]	0.2939 [0.2944]	
8	44–39–17	As-solidified	720	$\gamma' + \beta_1 + \beta_2$		0.3575 [0.3573]	0.2904 [0.2899]	0.2939 [0.2933]	
		1523 K	938	$\beta_1 + \beta_2$			0.2904	0.2920‡ [0.2921]	
		1273 K	644	$\gamma' + \beta_1 + \beta_2$		0.3576 [0.3575]	0.2909†	0.2943 [0.2944]	

(γ') γ' precipitated from quenching/cooling.
*X-ray data indicate that another phase, possibly an oxide, may be present.
†Measurement prone to error.
‡See text; extrapolation of β_2 phase boundary at 1523 K was based on these data.
§Few very weak lines for accurate measurement of lattice parameter.
[ ]calculated lattice parameter [21, 22].

TABLE II Analysed alloy and phase compositions and phase volume fractions

Alloy no.	Alloy composition determined by EPMA (at %) Ni–Al–Ru	Alloy treatment	Phases present	Phase composition determined by EPMA (at %), Ni–Al–Ru					
				γ	γ' (based on Ni_3Al)	β_1 (based on NiAl)	β_2 (based on RuAl)	$\beta_1 + \beta_2$*	(Ru)
1	71.4–18.3–10.3	As-solidified	$\gamma + \gamma' + \beta_1$ (90–5–5)	72.0–17.1–10.9†	‡	‡			
	71.0–18.6–10.4	1523 K	$\gamma + (\gamma') + \beta_1 + \beta_2$ (90–5–5)	73.8–16.7–9.5				38.8–38.7–22.5	
	70.2–19.0–10.8	1273 K	$\gamma + \gamma' + \beta_2$ (82–3–15)	76.3–15.4–8.3	73.1–21.9–5.0		24.0–45.2–30.8		
2	60.3–29.2–10.5	As-solidified	$\gamma' + \beta_1 + \beta_2$ (35–60–5)		69.9–24.7–5.4§	57.3–30.9–11.8†	32.6–42.5–24.9§		
	59.8–29.3–10.9	1523 K	$\gamma + (\gamma') + \beta_1$ (15–85)	76.1–18.0–5.9		57.1–31.0–11.9			
	59.5–29.6–10.9	1273 K	$\gamma' + \beta_2$ (70–30)		72.4–24.3–3.3		23.8–45.1–31.1		
3	49.3–24.6–26.1	As-solidified	$\gamma + \beta_2$ (65–35)	52.0–16.5–31.5†			24.1–41.8–34.1		
	48.2–25.6–26.2	1523 K	$\gamma + \beta_2 + (Ru)$ (62–35–3)	62.7–14.0–23.3			25.4–43.1–31.5		14.1–2.3–83.6§
	48.5–25.7–25.8	1273 K	$\gamma + \beta_2 + (Ru)$ (55–30–15)	72.9–14.5–12.6			24.0–43.7–32.3		9.5–1.3–89.2
4	24.3–24.6–51.1	As-solidified	$\gamma + \beta_2 + (Ru)$ (5–45–50)	48.5–16.6–34.9			17.2–43.4–39.4		28.9–11.5–59.6†
	25.2–24.7–50.1	1523 K	$\gamma + \beta_2 + (Ru)$ (10–50–40)	62.1–14.0–23.9			24.8–43.2–32.0		11.9–3.0–85.1
	24.7–25.6–49.7	1273 K	$\gamma + \beta_2 + (Ru)$ (15–50–35)	72.6–14.9–12.5			23.1–44.5–32.4		9.5–0.9–89.6
5	72.1–22.4–5.5	As-solidified	$\gamma' + \beta_1$ (90–10)		75.5–19.4–5.1†	63.7–28.6–7.7			
	72.3–22.4–5.3	1523 K	$\gamma + \gamma' + \beta_1$ (65–15–20)	77.5–17.9–4.6	75.2–22.1–2.7	60.5–30.0–9.5			
	72.1–22.4–5.5	1273 K	$\gamma' + \beta_2$** (80–20)		72.9–22.3–4.8		23.8–44.8–31.4		
6	67.6–27.2–5.2	As-solidified	$\gamma' + \beta_1$ (15–85)		75.4–22.1–2.5	65.1–28.7–6.2†			
	66.6–27.4–6.0	1523 K	$\gamma' + \beta_1$ (50–50)		74.5–23.4–2.1	60.6–30.3–9.1			
	65.8–27.8–6.4	1273 K	$\gamma' + \beta_2$ (70–30)		73.1–24.2–2.7		24.5–45.4–30.1		
7	29.3–46.4–24.3	As-solidified	$\gamma' + \beta_1 + \beta_2$ (2–15–83)		75.7–21.2–3.1	44.6–39.9–15.5	24.9–48.0–27.1†		
	29.9–45.9–24.2	1523 K	$\beta_1 + \beta_2$ (30–70)			35.2–44.5–20.3	27.2–46.4–26.4		
	30.3–46.3–23.4	1273 K	$\beta_1 + \beta_2$ (50–50)			34.1–45.8–20.1	23.9–47.3–28.8		
8	45.2–38.3–16.5	As-solidified	$\gamma' + \beta_1 + \beta_2$ (5–35–60)		76.6–19.8–3.6	45.6–39.3–15.1	29.7–44.9–25.4†		
	45.3–37.3–17.4	1523 K	$\beta_1 + \beta_2$					45.3–37.3–17.4	
	44.6–37.8–17.6	1273 K	$\gamma' + \beta_1 + \beta_2$ (40–5–55)		73.1–24.7–2.2	¶	24.1–46.4–29.5		

*Denotes compositions of phase mixture.
†Primary phase in the as-solidifed state; compositions represent centre of dendrites where appropriate.
‡Analysis not done (interdendritic composition 70Ni–22Al–8Ru (at %).
§Analysis prone to error.
¶Analysis could not be done due to small particle size.
**The tie line indicates a smaller proportion of β_2 than appears from the microstructure suggesting overall equilibrium has not been reached during annealing at 1273 K.
( )Approximate phase volume fraction in sequence.

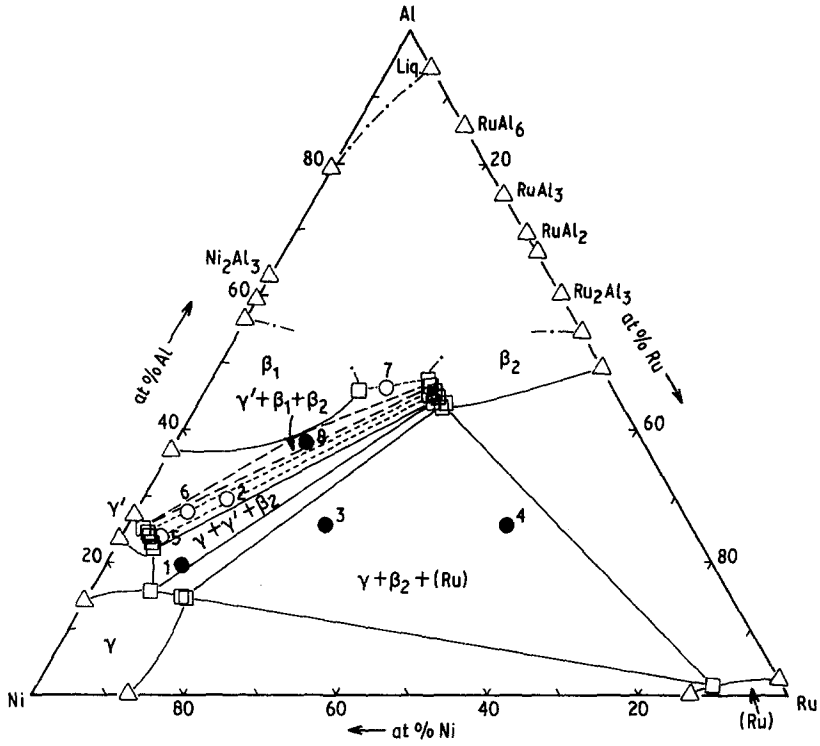

Figure 2 Partial isothermal section of the Ni–Al–Ru system at 1273 K. For key see Fig. 1.

4.1. Isothermal sections at 1523 K (Fig. 1)

The γ-phase region is extensive, reaching its limit at ~14 at % Al, 24 at % Ru, whereas the (Ru) region shows substantial solubility for nickel, but only a small solubility for Al. γ' dissolves up to ~4 at % Ru; the γ/γ' tie line for alloy 5 indicates a slight preferential partitioning of ruthenium to the γ-phase. A miscibility gap between β_1 and β_2 was found, in contrast to the assumption previously made [19]; however, the limits of the β_1 and β_2 regions have not been fully determined. Tie-line data were obtained for alloy 7 but in the case of alloys 1 and 8 metallographic contrast and EPMA data for β_1 and β_2 individually were not obtainable. From the β_2 lattice parameter measurements, the lower values for alloys 1 and 8 as compared with alloy 3 (Table I) indicate a greater nickel content [20] (see section 4.4), since nickel, having a smaller atomic diameter than ruthenium in solution is expected to decrease the RuAl parameter. The NiAl–RuAl relationships at higher aluminium contents than alloy 7 are not established; the present evidence does not rule out the possibility of the miscibility gap closing and being bounded by a region where β_1 and β_2 are fully intersoluble. EPMA data from alloys 2, 5 and 6 delineate the limits of β_1 at the aluminium-poor end of the region and are consistent with binary Ni–Al data [7–10].

Alloy 5 (Fig. 4a) provided identification of a $\gamma + \gamma' + \beta_1$ tie triangle and alloys 3 and 4 (Figs 5a and 6a) established an extensive $\gamma + \beta_2 +$ (Ru) tie triangle. The phase volume fractions were generally in reasonable agreement with the compositional data. The lattice parameters of the γ, β_2 and (Ru) in alloy 3 were essentially the same as the corresponding values in alloy 4, consistent with the tie-triangle determination. The presence of a $\gamma + \beta_1 + \beta_2$ tie-triangle was deduced from X-ray diffraction examination of alloy 1, but in this alloy the β_1 and β_2 phases were not distinguished from one another metallographically or by EPMA.

4.2. Isothermal section at 1273 K

The γ and (Ru) regions were smaller in extent than in the 1523 K isothermal section and the solubility of ruthenium in γ' (~5 at %) was slightly increased. Alloy 1 illustrates the preferential partitioning of ruthenium to γ. The EPMA data for all the alloys clearly locate the limit of the β_2 phase at ~25 at % Ni and ~43 to 47 at % Al at 1273 K; this limit agrees closely with the data from alloys 3, 4 and 7 at 1523 K, but the higher solubility value at ~40 at % Al, 35 at % Ni is indicated by the X-ray data for alloys 1 and 8 at 1523 K (Section 4.4). The solubility of ruthenium in NiAl at ~45 at % Al is ~20 at %, which is the same as the value at 1523 K; the extent of the β_1 field in the lower aluminium end of the range was reduced as compared with 1523 K.

The $\gamma + \beta_2 +$ (Ru) tie triangle (alloys 3 and 4) showed signficantly different compositions for γ and (Ru), respectively, compared with 1523 K, as a result of the decreased solubilities. Figs 5b and 6b shows the structure of alloys 3 and 4; in the case of alloy 3 a substantially greater proportion of (Ru) is present than that at 1523 K.

The most significant change at 1273 K is the replacement of the three-phase equilibria $\gamma + \gamma' + \beta_1$ and $\gamma + \beta_1 + \beta_2$ by equilibria involving $\gamma' + \beta_1 + \beta_2$ and $\gamma + \gamma' + \beta_2$. This change indicates the occurence of an invariant reaction at a temperature between 1523 and 1273 K; from the relationships of the three-phase equilibria (Fig. 7) the reaction is deduced to be $\gamma + \beta_1 \rightarrow \gamma' + \beta_2$. Microscopical features associated with the change of equilibria from 1523 to 1273 K are illustrated by alloys 1, 2, 5, 6, 8 (e.g. Figs 4, 8 to 10).

Alloys 2, 5 and 6 at 1523 K consist of $\gamma + \beta_1$, $\gamma + \gamma' + \beta_1$ and $\gamma' + \beta_1$, respectively (e.g. Figs 4a,

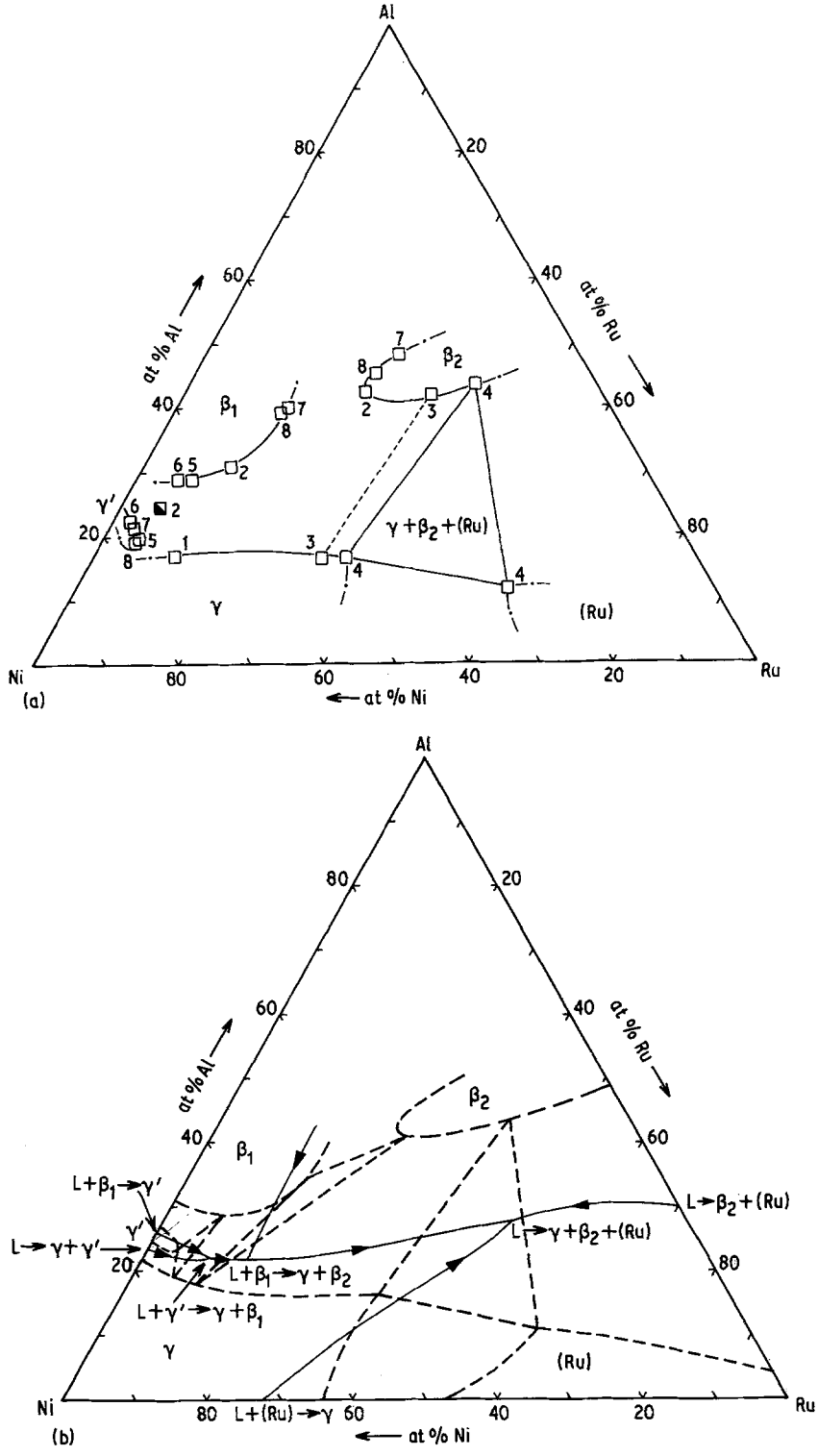

Figure 3 (a) Experimental phase compositional data from as solidified Ni–Al–Ru alloys. (□) phase compositions by EPMA with corresponding alloy numbers. (◪) γ' composition of alloy 2; analysis prone to error. (–·–·–) interpolated/extrapolated phase boundary. (—) three-phase region determined by EPMA. (-----) lines joining the composition of γ and β_2 as determined by EPMA. (b) Semi-schematic representation of liquidus and solidus projections based on binary phase diagrams (e.g. [7–10, 12–16]) and experimental ternary observations, assuming the following invariant reactions: $L + \gamma' \rightarrow \gamma + \beta_1$, $L + \beta_1 \rightarrow \gamma' + \beta_2$, $L \rightarrow \gamma + \beta_2 + (Ru)$. (→) liquidus curve; (---) solidus curve.

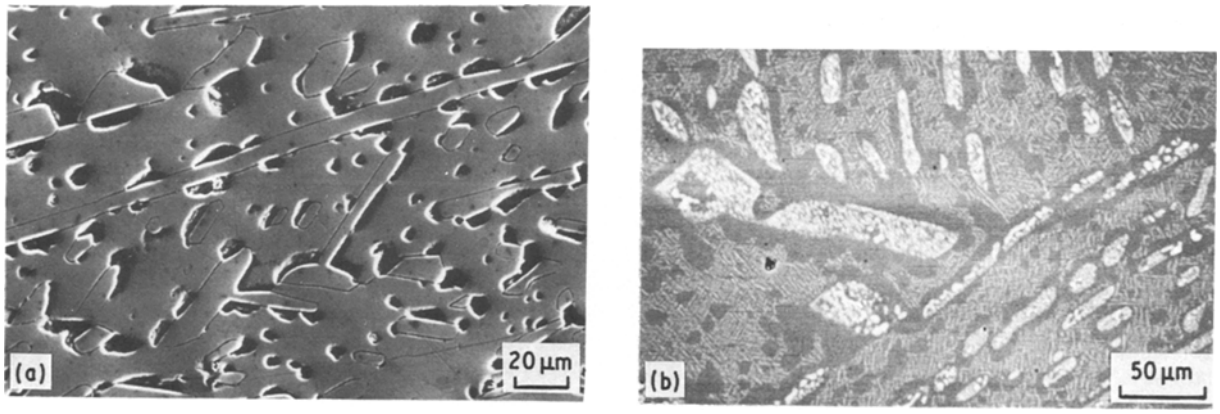

Figure 4 Alloy 5 (Ni–23Al–5Ru). (a) 1523 K. γ' (dark) and plates of β_1 (light) in γ matrix (grey). SEM, unetched. (b) 1273 K. β_2 (white) with γ' (dark). Regions of β_1 and γ at 1523 K have transformed into $\gamma' + \beta_2$. High resolution back-scattered electron image (HRBEI), unetched.

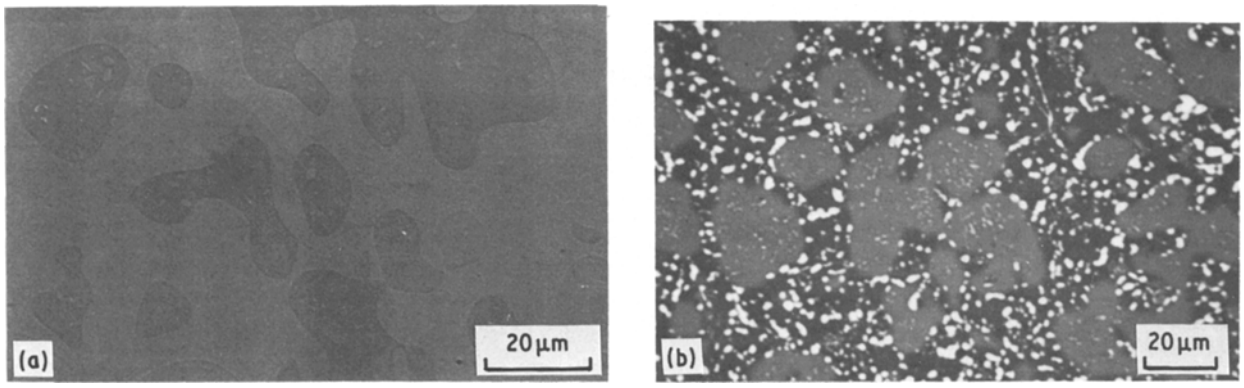

Figure 5 Alloy 3 (Ni–25Al–25Ru). (a) 1523 K. β_2 (dark) with fine precipitates of (Ru) within a matrix of γ (grey). Low resolution back-scattered electron image (LRBEI), unetched. (b) 1273 K. β_2 (grey) with γ (dark). (Ru) (white) has precipitated primarily in the γ region. HRBEI, unetched.

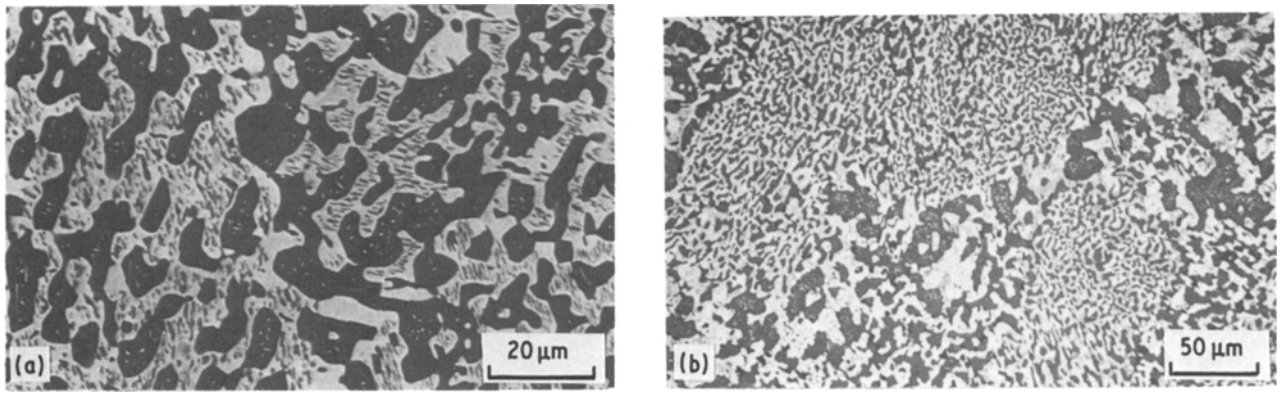

Figure 6 Alloy 4 (Ni–25Al–50Ru). Eutectic distribution of phases derived from as-solidified state is seen (Fig. 13). (a) 1523 K. β_2 (dark) with (Ru) (light) and γ (grey). Solid state precipitation of (Ru) within the β_2 can be seen. HRBEI, unetched.

9a); after annealing at 1273 K all three alloys consist of $\gamma' + \beta_2$ (Figs 4b, 8, 9b). The transformation involves the precipitation of β_2 in regions of γ and β_1 with the accompanying formation of γ', ie. $\gamma \rightarrow \gamma' + \beta_2$ and $\beta_1 \rightarrow \gamma' + \beta_2$. In alloy 8 annealed at 1523 K β_1 and β_2 were not distinguished from one another by metallography or EPMA but the structure is expected to be predominantly β_1. However, after annealing at 1273 K a lamellar structure formed, consisting of plates of γ' in a matrix of β_2 with a small proportion of β_1 particles (Fig. 10). The morphology suggests a discontinuous type reaction: $\beta_1 \rightarrow \gamma' + \beta_2$.

The presence of a three phase region $\gamma + \beta_2$(RuAl) + (Ru) at 1273 and 1523 K is in agreement with previous work [18]. The observation of $\gamma + \gamma' + \beta_2$ and $\gamma' + \beta_1 + \beta_2$ regions at 1273 K differs from the previously reported equilibria $\gamma + \gamma' + \beta_1$ and $\gamma' + \beta_1 + \beta_2$ at 873 K [18]. Considering the present results in relation to the previous work [18], an increase in the extent of the $\beta_1 + \beta_2$ miscibility gap is seen with decrease in temperature.

4.3. Solidification behaviour

Fig. 3 shows a possible form of the liquidus projection for the system based on binary diagram information and observations on the as-solidified and also the annealed ternary alloys. Phase compositional data from the as-solidified alloys are included for correlation with solidus features.

The liquidus depicted involves three ternary invariant reactions $L + \gamma' \rightarrow \gamma + \beta_1$; $L + \beta_1 \rightarrow \gamma + \beta_2$; $L \rightarrow \gamma + \beta_2 +$ (Ru).

Alloys 1 and 3 show primary γ, alloy 5 primary γ', alloys 2 (Fig. 11) and 6 primary β_1 and alloys 4, 7 and 8 primary β_2 (e.g. Figs 12, 13). The structure of alloy 4 is essentially eutectic in nature showing both coarse and fine regions (Fig. 13); the former are interpreted as a binary eutectic mixture of β_2 + (Ru) and the latter as a ternary eutectic of β_2 + (Ru) + γ containing only a small proportion of γ.

The three-phase reaction involving liquid, β_1 and β_2 is deduced from observations on alloys 7 and 8 [20]. β_2 is the primary phase in both alloys, the volume

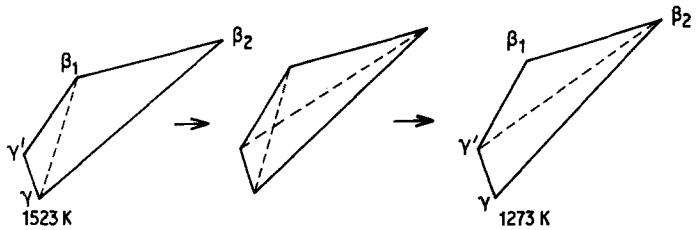

Figure 7 Schematic representation of invariant reaction $\gamma + \beta_1 \rightarrow \gamma' + \beta_2$ at a temperature between 1523 and 1273 K.

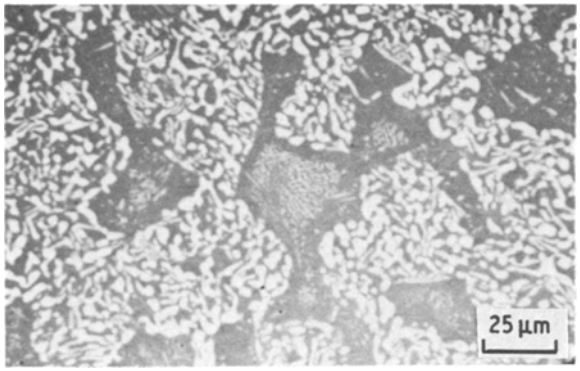

Figure 8 Alloy 2 (Ni–30Al–10Ru), 1273 K. β_2 (light), γ' (dark). β_1 and γ regions originally present at 1523 K have transformed to β_2 and γ'. The areas showing coarser β_2 formed from the γ areas by the reaction $\gamma \rightarrow \beta_2 + \gamma'$; the finer dispersion of β_2 formed from the β_1 areas by the reaction $\beta_1 \rightarrow \beta_2 + \gamma'$.

fraction being greater in alloy 7, consistent with the greater ruthenium content of the alloy. Duplex eutectic structures were not observed, but a divorced eutectic reaction liquid $\rightarrow \beta_1 + \beta_2$ is a possibility with the liquid composition lying close to that of β_1. The occurrence of a peritectic: liquid $+ \beta_2 \rightarrow \beta_1$ appears the most likely interpretation of the observations. The presence of small amounts of γ' in the as-solidified alloys 7 and 8 is interpreted as resulting from non-equilibrium solidification; the peritectic would not proceed to completion and liquid then deposits β_1 and the liquid composition is assumed to change over the β_1 liquidus surface until it encounters the $L + \beta_1 \rightarrow \gamma'$ reaction curve when γ' formation occurs.

4.4. Lattice parameter data

In the annealed alloys 1 to 5 the aluminium contents of the γ-phase lie between 14 and 18 at % and there is a linear increase (Fig. 14) between lattice parameter and ruthenium content of the γ; calculated values of parameter, using ruthenium atomic radius and Ni–Al binary data [21] are in good agreement with the measured values [22]. Observed expansion of the lattice by ruthenium agrees well with results for Ni–Ru alloys [23]. The parameters of γ' in equilibrium with γ lie between 0.3575 and 0.3577 nm reflecting the small variation of γ' composition; calculated values agree well with those measured.

Where γ and γ' coexist in equilibrium (alloy 1: 1273 K and alloy 5: 1523 K) the lattice parameter mismatch values are very small, -0.23 and $+0.08\%$, respectively. In alloys 1 and 2 annealed at 1523 K some γ' forms during quenching, with a very small negative mismatch.

For β_2 phase the lattice parameter values in alloys 1 to 8 all lie between 0.2946 and 0.2949 nm after annealing at 1273 K, consistent with the relatively small differences in aluminium and nickel content of the phase (Fig. 2). After annealing at 1523 K, alloys 1, 3, 4, 7 and 8 contained β_2 and in alloys 3 and 4 the phase parameters and compositions are effectively the same as after treatment at 1273 K; also alloy 7 showed little change from 1273 K. However, in alloys 1 and 8 the β_2 parameter was reduced to ~ 0.292 nm; no compositional data were obtained for the β_2 for these cases, but the lower value is interpreted as deriving from an increased solubility of nickel in β_2, as depicted in Fig. 1. Calculated values (Table II) of β_2 parameter assuming a value of 0.303 nm for binary RuAl, agree reasonably with the measured data [21, 22].

The lattice parameter values for β_1 are lower than for β_2, lying between 0.2873 and 0.2936 nm. Calculated values taking into account the dependence of binary NiAl parameter on aluminium content agree reasonably with the experimental data [21]. In previous work [18] on the 873 K isothermal section, the parameter of the NiAl based solid solution was shown as being greater than that of RuAl based solution.

The parameter mismatch values between coexisting β_1 and β_2 are low, i.e. $< 0.6\%$ (Table II). The presence of the $\beta_1 + \beta_2$ miscibility gap, even with this small mismatch suggests that features other than "size factor" limit the extent of mutual solubility.

In the hexagonal (Ru) solid solution phase, the values of c and a are less than in pure ruthenium and decrease with increasing content of nickel in solution as expected from atomic radius considerations. The data for alloys 3 and 4 are shown in Fig. 15 as a function of nickel in (Ru) and ignoring variations in aluminium content of (Ru).

4.5. Hardness data

Hardness values in the series of alloys studied range from 220 to 940 H_v. The differences between individual alloys and treatments can be discussed qualitatively in

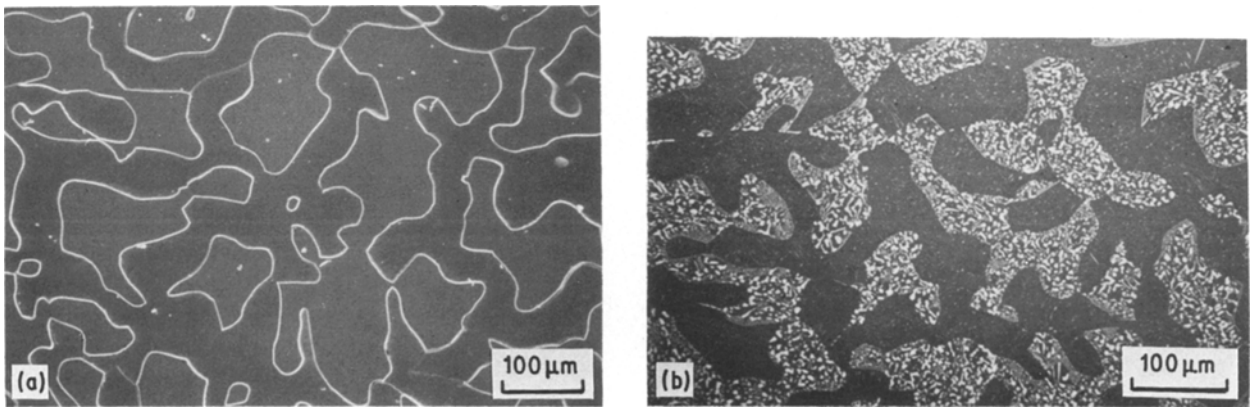

Figure 9 Alloy 6 (Ni–28Al–5Ru). (a) 1523 K. β_1 (dark), γ' (grey). SEM, etched in HF + HNO_3 + H_2O. (b) 1273 K. γ' (dark), β_2 (white). The original β_1 region at 1523 K has transformed: $\beta_1 \rightarrow \beta_2 + \gamma'$. Some precipitates of β_2 within γ' are also evident. HRBEI, unetched.

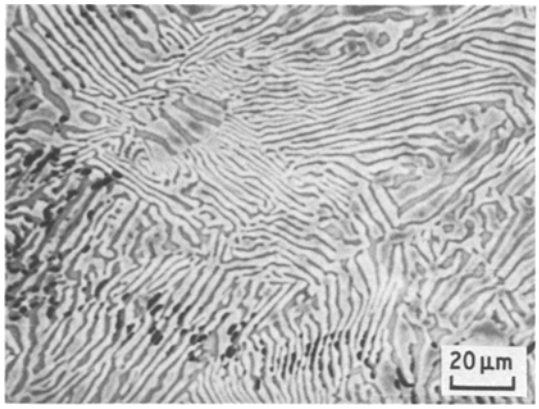

Figure 10 Alloy 8 (Ni–39Al–17Ru), 1273 K. γ' lamellae (light), β_2 (grey) and some particles of β_1 (dark). HRBEI, electrolytically etched in NaOH.

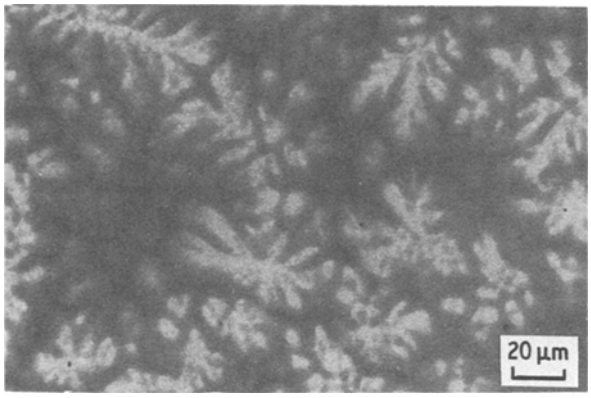

Figure 11 Alloy 2 (Ni–30Al–10Ru), as solidified. β_1 dendrites (light) containing precipitates of β_2 (grey) with γ' (dark) in the interdendritic regions. HRBEI, unetched.

terms of the inherent hardness values of the phases (which are influenced by phase composition) and by the phase volume fractions and dispersions.

Typical microhardness values of ~285 and ~270 H_v were found for γ and γ', respectively, in alloys 1, 2, 3, 5, 6. Alloys 1 and 5 are dominated by γ and/or γ' and show relatively low values from 220 to 360 H_v. Alloys 2 and 6 consists of two or three-phase combinations of γ', β_1 and β_2; the relatively high as-solidified hardness levels may depend partly on a fine phase dispersion, while the high volume fraction of β_1 in alloy 2 annealed at 1523 K is the likely cause of the high hardness.

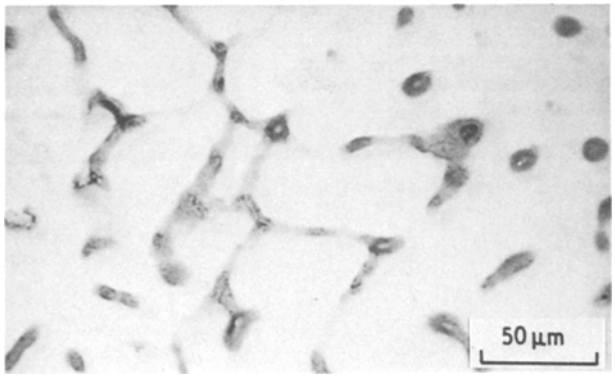

Figure 12 Alloy 7 (Ni–50Al–22Ru), as solidified. Primary dendrites of β_2 (white) and interdendritic regions of β_1 (grey) containing precipitates of γ' (dark). HRBEI, etched in HF + HNO_3 + H_2O.

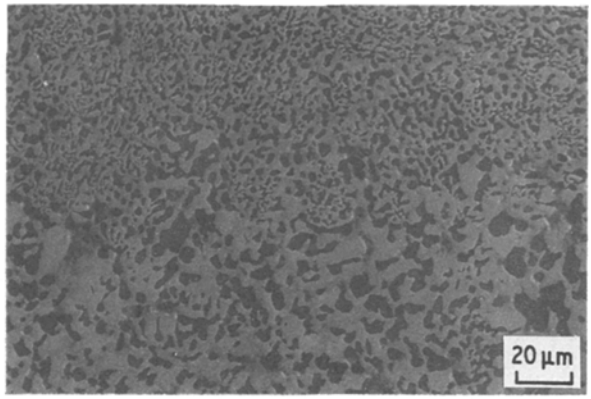

Figure 13 Alloy 4 (Ni–25Al–50Ru), as solidified. Binary and ternary eutectic morphologies with (Ru) (light), β_2 (dark) and γ (grey). Ternary eutectic (Ru) + β_2 + γ (average composition Ni–27.8Al–51.5Ru) is the region with coarser particles; the binary eutectic of (Ru) + β_2 (average composition Ni–25.7Al–52.9Ru) is the region with finer particles. SEM, unetched.

Alloys 3 and 4 consist of $\gamma + \beta_2$ and $\gamma + \beta_2$ + (Ru), respectively, in the as-solidified state. The very high hardness in alloy 4 (~690 to 880 H_v) is interpreted as due to the substantial proportions of β_2 and of (Ru). The microhardness of (Ru) was found to be ~780 H_v. The highest hardness in alloy 4 is shown by the as-solidified condition and the value decreases with decrease in annealing temperature; this may be interpreted as due to a decrease in nickel in solution in (Ru) with a consequent reduction in solid solution hardening.

In alloys 7 and 8 (with the exception of the 1273 K state in alloy 8), the structures consist wholly or predominantly of $\beta_1 + \beta_2$ and have hardness values ~720 to 940 H_v. The highest value 940 H_v (alloy 8, 1523 K) is associated with the higher degree of nickel solubility in RuAl (Fig. 1 and Table I); the relatively low value of ~640 H_v in alloy 8 annealed at 1273 K is

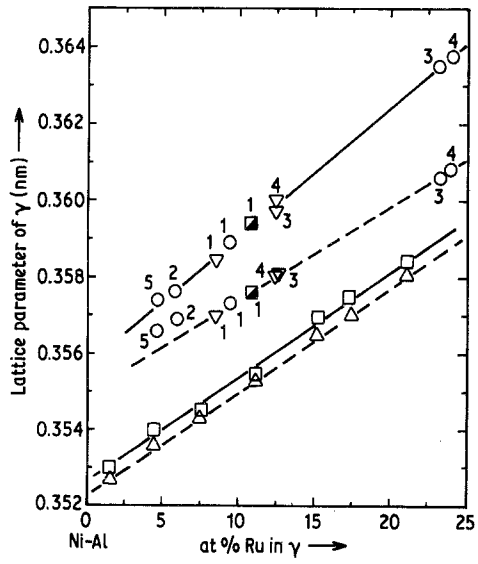

Figure 14 Plots of γ-phase lattice parameter against ruthenium content of γ for alloys 1 to 5 and binary Ni–Ru alloys [23]. As-solidified data for alloys 3 and 4 are omitted since error is expected in the analysis of the γ regions. (—) experimentally determined parameter. (– – –) corresponding calculated parameter based on [21, 22]. (○) 1523 K; (▽) 1273 K; (◪), as-solidified. (□) experimental data on binary Ni–Ru alloys [23]. (△) corresponding calculated values [21, 22].

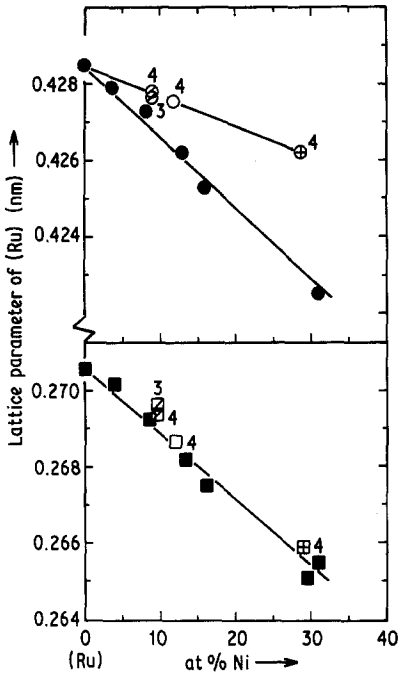

Figure 15 Plots of c and a lattice parameters for (Ru) against nickel content of (Ru) in alloys 3 and 4 assuming contant aluminium content. Experimental data on binary (Ru) from [23] are also shown. (○, ⊘, ⊕) data for c-axis of (Ru) at 1523, 1273 K and as-solidified state, respectively. (●) data for c-axis of (Ru) from [23]. (□, ⊡, ⊞) data for a-axis of (Ru) at 1523, 1273 K and as-solidified state, respectively. (■) data for a axis of (Ru) from [23].

interpreted as due to the substantial amount of softer γ'. In previous work on alloys annealed at 873 K [18], stoichiometric NiAl containing ~ 5 at % Ru and stoichiometric RuAl containing ~ 8 at % Ni, were reported as showing microhardness values of ~ 1000 and $\sim 750\,H_v$, respectively. In the present work, typical microhardness values of somewhat lower than these were found with β_2 being slightly harder than β_1, i.e. 770 and $680\,H_v$.

5. Conclusions

A miscibility gap exists between the solid solution of ruthenium in NiAl (designated β_1) and the solid solution of nickel in RuAl (designated β_2); observations show that the gap originates on solidification, probably by the reaction: liquid + $\beta_2 \rightarrow \beta_1$. The lattice parameter mismatch between β_1 and β_2 coexisting in equilibrium is small, i.e. $\leqslant \sim 0.6\%$. The γ'-phase dissolves up to ~ 5 at % Ru and shows a very small lattice mismatch with γ-phase (Tables I and II).

The liquidus is proposed to contain three invariant reactions: L + $\gamma' \rightarrow \gamma + \beta_1$, L + $\beta_1 \rightarrow \gamma + \beta_2$ and L $\rightarrow \gamma + \beta_2$ + (Ru). In the solid state an invariant reaction occurs between 1523 and 1273 K, deduced to be $\gamma + \beta_1 \rightarrow \gamma' + \beta_2$.

Acknowledgements

We wish to thank SERC for support of the work, Johnson Matthey Research Centre for the provision of ruthenium, and Professor D. W. Pashley FRS for the provision of research facilities.

References

1. R. G. WING and I. R. McGILL, *Platinum Met. Rev.* **25** (1981) 2.
2. M. R. JACKSON and J. R. RAIRDEN, *Met. Trans.* **8A** (1977) 1697.
3. E. J. FELTEN, *Oxid. Met.* **10** (1976) 23.
4. C. W. CORTI, D. R. COUPLAND and G. L. SELMAN, *Platinum Met. Rev.* **24** (1980) 2.
5. *Idem,* Proceedings of the Conference on "Behaviour of High Temperature Alloys in Aggressive Environments", Petten, The Netherlands (1979).
6. A. S. DARLING and M. McLEAN, Brit. Pat. JX/5282/02, 50597/77.
7. M. HANSEN and K. ANDERKO, "Constitution of binary alloys", 2nd Edn (McGraw Hill, New York, 1958) p. 118.
8. R. P. ELLIOTT, *ibid.,* 1st supplement (1965) p. 48.
9. F. A. SHUNK, *ibid.,* 2nd supplement (1969) p. 31.
10. P. NASH and D. R. F. WEST, *Met. Sci.* **17** (1983) 99.
11. A. TAYLOR and A. J. DOYLE, *J. Appl. Cryst.* **5** (1972) 201.
12. P. NASH, Bull Alloy Diagrams (unpublished work, Illinois Institute of Technology).
13. N. I. VARICH and A. N. PETRUNINA, *Russ. Met. (Metally)* **2** (1979) 90.
14. W. OBROWSKI, *Naturwiss.* **47** (1960) 14.
15. *Idem, Metall* **17** (1963) 108.
16. A. MAGNÉLLI, L. E. EDSHAMMAR, T. DAGERHAMN and S. WESTMAN, Final Technical Report No. I on contract DA-91-591-EUC-3134 (AD 451442) (1964) p. 6.
17. L. E. EDSHAMMAR, *Acta Chem. Scand.* **20** (1966) 427.
18. V. F. TSURIKOV, E. M. SOKOLOVSKAYA, and E. F. KAZAKOVA, *Vestnik Moskovskogo Universiteta, Khimiya.* **35** (1980) 512.
19. S. CHAKRAVORTY, H. HASHIM and D. R. F. WEST, *J. Mater. Sci.* **20** (1985) 2313.
20. S. CHAKRAVORTY and D. R. F. WEST, *Scripta Metall.* **19** (1985) 1355.
21. A. J. BRADLEY and A. TAYLOR, *Proc. R. Soc.* **A159** (1937) 56.
22. S. CHAKRAVORTY and D. R. F. WEST, *Mater. Sci. Tech.* **1** (1985) 61.
23. I. I. KORNILOV and K. P. MYASNIKOVA, *Izv. Akad. Nauk. SSSR, Met. i. Gornoe Delo* **4** (1964) 159; (English translation: Russ. Met. Mining 4 (1964) 95).

Received 27 August
and accepted 4 October 1985